Ca^{2+}-Induced Increased Lipid Packing and Domain Formation in Submitochondrial Particles. A Possible Early Step in the Mechanism of Ca^{2+}-Stimulated Generation of Reactive Oxygen Species by the Respiratory Chain†

Mercedes T. Grijalba,‡ Anibal E. Vercesi,§ and Shirley Schreier*,‡

Department of Biochemistry, Institute of Chemistry, Universidade de São Paulo, C.P. 26077, CEP 05599-970 São Paulo, SP, Brazil, and Department of Clinical Pathology, Medical School, Universidade Estadual de Campinas, C.P. 6109, CEP 13083-970 Campinas, SP, Brazil

Received December 4, 1998; Revised Manuscript Received June 7, 1999

ABSTRACT: Ca^{2+} and P_i accumulation by mitochondria triggers a number of alterations leading to nonspecific increase in inner membrane permeability [Kowaltowski, A. J., et al. (1996) *J. Biol. Chem. 271*, 2929−2934]. The molecular nature of the membrane perturbation that precedes oxidative damage is still unknown. EPR spectra of spin probes incorporated in submitochondrial particles (SMP) and in model membranes suggest that Ca^{2+}−cardiolipin (CL) complexation plays an important role. Ca^{2+}-induced lipid domain formation was detected in SMP but not in mitoplasts, in SMP extracted lipids, or in CL-containing liposomes. The results were interpreted in terms of Ca^{2+} sequestration of CL tightly bound to membrane proteins, in particular the ADP−ATP carrier, and formation of CL-enriched strongly immobilized clusters in lipid shells next to boundary lipid. The in-plane lipid and protein rearrangement is suggested to cause increased reactive oxygen species production in succinate-supplemented, antimycin A-poisoned SMP, favoring the formation of carbon-centered radicals, detected by EPR spin trapping. Removal of tightly bound CL is also proposed to cause protein aggregation, facilitating intermolecular thiol oxidation. Lipid peroxidation was also monitored by the disappearance of the nitroxide EPR spectrum. The decay was faster for nitroxides in a more hydrophobic environment, and was inhibited by butylated hydroxytoluene, by EGTA, or by substituting Mg^{2+} for Ca^{2+}. In addition, Ca^{2+} caused an increase in permeability, evidenced by the release of carboxyfluorescein from respiring SMP. The results strongly support Ca^{2+} binding to CL as one of the early steps in the molecular mechanism of Ca^{2+}-induced nonspecific inner mitochondrial membrane permeabilization.

Mitochondrial Ca^{2+} overload can lead to a state of nonspecific inner membrane permeability termed mitochondrial permeability transition (MPT)[1] (*1*). Ca^{2+}-loaded respiring mitochondria exhibit an increase in the ROS production, followed by enhanced lipid and protein oxidation (*2*−*7*), culminating in increased membrane permeability (*1*, *2*, *8*). This effect is potentiated by a series of compounds such as P_i, arsenate, thiol reagents, prooxidants, and uncouplers (*1*−*5*). MPT is characterized by the opening of a cyclosporin A-sensitive proteinaceous pore (mitochondrial permeability transition pore) that leads to mitochondrial uncoupling, swelling, Ca^{2+} efflux, and loss of matrix components, including proteins (*1*,*8*). Evidence has been presented that MPT, a lethal condition to the cell, is related to pathological states, such as ischemia-reperfusion (*4*, *6*, *9*, *10*). In addition, during prolonged ischemia, the intracellular Ca^{2+} rises to levels sufficient to cause mitochondrial Ca^{2+} accumulation upon reoxygenation (*10*). Under this condition, short-lived free radicals such as superoxide (O_2^{-}), hydroxyl ($HO^{\bullet}$), and lipid peroxides ($ROO^{\bullet}$) are produced (*9*, *10*). Much data strongly indicates that the opening of the MPT pore is mediated by a Ca^{2+}-stimulated generation of reactive oxygen species (ROS) (*2*−*7*), suggesting that Ca^{2+} and ROS have a synergistic action in the pathophysiology of tissue injury during post-ischemic myocardial reperfusion (*3*, *6*, *9*). Despite many studies, the precise nature of mitochondrial membrane perturbation and the role of Ca^{2+} at a molecular level are not well understood.

Cardiolipin (CL) is essentially the only negatively charged phospholipid, mainly found in the inner monolayer, of the inner mitochondrial membrane (IMM) of eukaryotic cells

† This research was supported by grants from Fundação de Amparo à Pesquisa no Estado de São Paulo (FAPESP) and Conselho Nacional de Desenvolvimento Científico e Tecnológico (CNPq), by a FAPESP postdoctoral fellowship to M.T.G., and by CNPq research fellowships to A.E.V. and S.S.

* To whom correspondence should be addressed: Department of Biochemistry, Institute of Chemistry, Universidade de São Paulo, Brazil. Phone and fax: +55-11-818-2179. E-mail: schreier@iq.usp.br.

‡ Universidade de São Paulo.

§ Universidade Estadual de Campinas.

[1] Abbreviations: AAC, ADP−ATP carrier; BHT, butylated hydroxytoluene; CL, cardiolipin; CF, carboxyfluorescein; COX, cytochrome *c* oxidase; DCP, dicetyl phosphate; DMPO, 5,5-dimethyl-1-pyrroline *N*-oxide; IMM, inner mitochondrial membrane; MPT, mitochondrial permeability transition; PC, egg phosphatidylcholine; 5-PCSL, 1-palmitoyl-2-stearoyl-(5-doxyl)-*sn*-glycero-3-phosphocholine; 7-PCSL, 1-palmitoyl-2-stearoyl-(7-doxyl)-*sn*-glycero-3-phosphocholine; ROS, reactive oxygen species; SSL, 4-(octadecanoylamino)-2,2,6,6-tetramethylpiperidine-1-oxyl; SMP, submitochondrial particles; TX-100, Triton X-100; 5-SASL, 5-doxylstearic acid; 5-MeSL, methyl ester of 5-doxylstearic acid; 12-SASL, 12-doxylstearic acid.

10.1021/bi9828674 CCC: $18.00
Published on Web 09/17/1999

(*11*). CL is tightly bound to various enzymes and protein complexes (*12*, *13*) involved in transport processes across the membrane, such as the ADP−ATP carrier (AAC; *14*), regulating their activities.

In model systems, CL undergoes a bilayer to hexagonal H_{II} phase transition in the presence of Ca^{2+} (*15*). In mixtures of anionic and zwitterionic phospholipids, Ca^{2+} can also induce lateral phase separation (lipid domain formation; *16*−*18*). It is believed that both processes are important for membrane functioning (*19*). However, only phase separation has been observed in biological systems (*17*), and its characterization in mitochondria is still lacking. The importance of the Ca^{2+}−CL interaction at the IMM level has been recognized on the basis of recent work proposing that this interaction is responsible for the Ca^{2+}-induced channel opening in liposomes containing AAC (*20*). Therefore, a mechanism involving this interaction could play an important role in various membrane deleterious processes induced by the disruption of mitochondrial Ca^{2+} homeostasis.

In this work, we present spectroscopic evidence for Ca^{2+}-induced changes of membrane molecular organization, very likely due to the interaction between the cation and CL. To examine this possibility, inverted bovine heart submitochondrial particles (SMP) were used. In this system, CL is predominantly located in the outer monolayer (*11*), facilitating the study of Ca^{2+} effects. Membrane lipid organization was assessed by analysis of the EPR spectra of spin probes containing the paramagnetic nitroxide moiety at different depths in the bilayer. Lipid peroxidation was evidenced by the loss of the EPR signal of the incorporated spin probes. Radical formation was assessed by the spin trapping technique. Permeability changes were detected by the leakage of a fluorescent probe [carboxyfluorescein (CF)] trapped in the SMP aqueous compartment.

MATERIALS AND METHODS

Materials. ATP, bovine heart CL, EGTA, Hepes, $MgCl_2$, $CaCl_2$, sucrose, sodium succinate, BHT, rotenone, DMPO, DCP, 5-SASL, 5-MeSL, and 12-SASL were from Sigma Chemical Co. 5-PCSL and 7-PCSL were from Avanti Polar Lipids, Inc. CF was from Eastman Kodak. SSL was synthesized by H. Dugas from the University of Montreal and was a gift of I. C. P. Smith (National Research Council of Canada). The other reagents were of the purest grade available. Milli Q water was used throughout.

Isolation of Bovine Heart Mitochondria and Preparation of SMP and Liposomes. Mitochondria were isolated according to ref *21*. SMP were obtained from frozen mitochondria (*22*). Lipid and protein contents were quantitated according to refs *23* and *24*, respectively. SMP lipids were extracted with $CHCl_3/CH_3OH$ (1:2, v/v) by the Folch procedure (*25*).

Incubation Procedure. SMP (1−2 mg of protein/mL) were incubated in 125 mM sucrose, 65 mM KCl, 0.5 mM ATP, 10 μM rotenone (unless otherwise specified), and 0.25−2.0 mM P_i (added after preincubation with Ca^{2+}) in 10 mM Hepes (pH 7.2). Energization was achieved by addition of succinate. EPR spectra were obtained after preincubation for 15 min with Ca^{2+} or Mg^{2+} at 32 °C. BHT, a chain-breaking antioxidant that scavenges propagating alkoxyl and peroxyl radicals formed during lipid peroxidation, was added as specified in the figure legends. When added to controls to form complexes with any spurious ions, EGTA was at a concentration of 1 mM. When EGTA was added to complex Ca^{2+} present in samples, its concentration was 2 or 3 times greater than that of the ion.

Spin Labeling and EPR Measurements. SSL, 5-SASL, 5-MeSL, and 12-SASL stock solutions were prepared in chloroform and stored at −15 °C. Appropriate volumes were dried under N_2; SMP suspensions were added and the mixtures gently stirred for 1 h at 4−6 °C. 5-PCSL and 7-PCSL were added in the form of concentrated ethanolic solutions. EPR measurements were taken within 4 h. For liposome preparation, lipids and spin label chloroform solutions were evaporated under a stream of N_2. The remaining solvent was removed under vacuum for 2 h. PC/20 mol % CL and PC/20 mol % DCP multilamellar liposomes were prepared upon addition of buffer to the lipid films followed by vortexing and bath sonication for 30 min at 4 °C.

The membrane lipid acyl chain degree of order was assessed by calculating effective order parameters (S_{eff}) from the EPR spectra of intercalated spin probes according to refs *26* and *27*. S_{eff} measures the amplitude of motion of the probe's long molecular axis in the bilayer. Membrane organization was also measured by the ratio of heights of the low-field (h_{+1}) to the center-field (h_0) resonances in the EPR spectra of 5-MeSL (*28*). This parameter contains the contribution of both order and mobility and expresses changes in overall membrane organization, lower h_{+1}/h_0 values being ascribed to a more organized bilayer. The appearance of an additional, more immobilized, component also causes a decrease in the h_{+1}/h_0 ratio (*28*). One mole percent probe was used to obtain spectra for the measurement of S_{eff} and the h_{+1}/h_0 ratio, as well as in the lipid peroxidation studies (see below).

Lateral phase separation was monitored by evaluating the extent of exchange broadening in samples with high probe concentrations. Under these conditions, exchange-broadened spectra are obtained due to the high probe collision frequency. Such spectra tend to display *c*/*d* ratios (measured in the low-field resonance, Figure 6A; *28*) close to or greater than 1. Lateral phase separation causes an increase in the exchange frequency due to an increase in spin probe local concentration, promoting additional line broadening and leading to an increase in the *c*/*d* ratio. Such an effect was observed in a study of Ca^{2+}-induced lateral phase separation (*16*). To observe the exchange interaction, 5−15 mol % probe was employed.

The kinetics of the reaction of spin-label with radicals generated during Ca^{2+}-mediated lipid peroxidation in respiring SMP were followed by monitoring the intensity of the center field line (h_0) in the nitroxide EPR spectra (*29*).

Spin Trapping. Oxygen and carbon free radicals were identified as DMPO adducts. EPR spectra were obtained in a Bruker ER-200D-SRC spectrometer at room temperature using flat quartz cells from Wilmad Glass Co., Inc.

Evaluation of Membrane Permeability by Carboxyfluorescein Fluorescence. The concentration-dependent self-quenching of CF fluorescence can be used to monitor the leakage of the dye incorporated in the aqueous compartment of SMP. CF (0.1 M) was added to the medium containing mitochondria prior to SMP preparation. External CF was removed by three sequential centrifugation steps at 100000*g* for 30 min at 4 °C. The suspension was exposed to variable

Ca^{2+} concentrations and supplemented with succinate, and the fluorescence intensity was measured. CF release, evidenced by a fluorescence increase, occurs due to an increase in permeability. Fluorescence measurements were taken in a SPEX-fluorog spectrofluorimeter at 32 °C, using a λ_{exc} of 479 nm and a λ_{em} of 520 nm; excitation slits were 0.1 and 0.1 mm, and emission slits were 0.1 and 0.1 mm.

RESULTS

Ca^{2+}-Induced Increase in Lipid Organization and Lateral Phase Separation in SMP. Ca^{2+} effects on IMM lipid organization were evaluated by analyzing the EPR spectra of intercalated spin probes bearing the nitroxide moiety at different depths in the bilayer. SSL, a derivative of stearamide, carries the paramagnetic group at the polar headgroup; therefore, it senses the membrane−water interface (*30*). The other labels have the *N*-oxyl oxazolidine moiety at carbons 5 (5-SASL, 5-MeSL, and 5-PCSL), 7 (7-PCSL), and 12 (12-SASL) of the acyl chain. The spin probes are either ionic (5-SASL and 12-SASL), zwitterionic (5-PCSL and 7-PCSL), or nonionic (SSL and 5-MeSL). Addition of Ca^{2+} caused alterations in the spectra of all spin probes, irrespective of the location of the nitroxide in the bilayer, indicating changes in the organization of the SMP lipid components. Two associated physical processes were detected, in a cation concentration-dependent manner: restricted lipid motion and increased molecular order, and lateral phase separation. All studies concerning the Ca^{2+} effects on lipid organization were performed with nonrespiring SMP to avoid loss of the EPR signal during respiration (see below).

EPR spectra were obtained for spin probes incorporated in SMP at low and high probe-to-lipid molar ratios. The results for low molar ratios will be presented first. Figure 1A shows that in the absence of Ca^{2+}, SSL exhibits a two-component spectrum, one corresponding to a weakly immobilized population (narrow triplet) and the other to a strongly immobilized population (broad triplet). Ca^{2+} promotes an intense probe immobilization, causing the disappearance of the weakly immobilized component (Figure 1B). This result is indicative of a pronounced increase in lipid packing. The fact that no loss of spin probes occurred was shown by solubilizing SMP in detergent (TX-100) and verifying that the double integrals of the spectra in the absence and in the presence of Ca^{2+}, as well as that of detergent-solubilized particles (that yield a narrow line triplet), are essentially the same (data not shown).

The spectra of 5-SASL, 5-PCSL, and 7-PCSL exhibited outer and inner extrema, allowing the calculation of order parameters, S_{eff} (Table 1). The large S_{eff} values in SMP are in agreement with the high protein content in these particles (75−80 wt %) (*11*, *12*). In this system, part of the lipid must be strongly immobilized due to lipid−protein interaction. Accordingly, smaller S_{eff} values were obtained for model systems consisting of PC/20 mol % CL and PC/20 mol % DCP (Table 1). Figure 2 shows that S_{eff} for 5-SASL in SMP increases with increasing Ca^{2+} concentrations. In Table 1, it is seen that Ca^{2+} caused an increase in S_{eff} for all the systems that were studied: SMP and model membranes containing negatively charged phospholipids (DCP or CL). The increase in the order parameter, indicative of a decrease in the amplitude of motion of the probe's long molecular axes, was observed both for phospholipid spin labels and for 5-SASL. Addition of EGTA prior to Ca^{2+} prevented the increase in S_{eff}. When Mg^{2+} was added instead of Ca^{2+}, only a slight motional freezing of the lipid acyl chains was observed both in SMP and in liposomes (Table 1).

The line shapes displayed by the probes described above render it difficult to detect two (or more) spectral components, indicative of the existence of lipid domains with

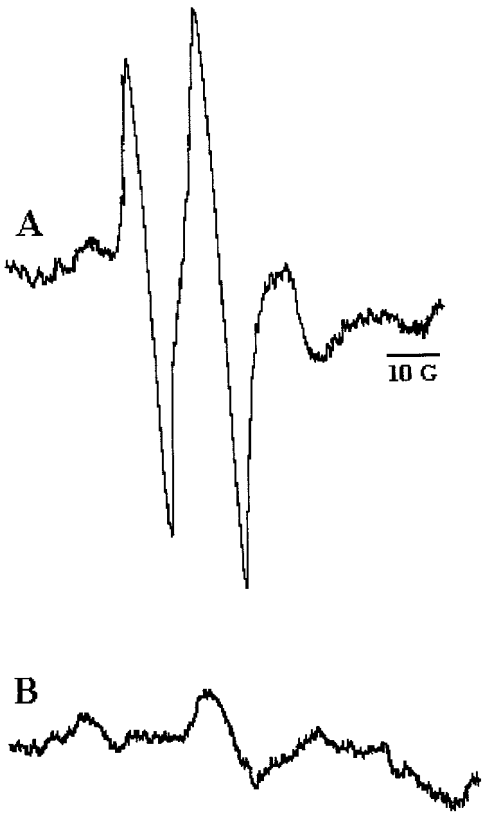

FIGURE 1: Effect of Ca^{2+} on the SMP lipid headgroup organization. EPR spectra of SSL (1 mol %) incorporated in SMP (1.5 mg of protein/mL) in standard medium (see Materials and Methods) containing 1.0 mM EGTA (top) and in the presence of 1.5 mM Ca^{2+} (bottom). Experimental conditions were as follows: power of 10 mW, modulation amplitude of 1.25 G, gain of 6.3×10^5, and spectral scan width of 100 G.

Table 1: Ca^{2+} Effect on the Order Parameter, S_{eff}, and on the h_{+1}/h_0 Ratio Measured in the EPR Spectra of Spin Probes Incorporated in SMP and in Model Systems (2 mM total lipid)

		S_{eff}		
system	probe	EGTA[a]	Ca^{2+}	Mg^{2+}
SMP (2.0 mg of protein/mL)	5-PCSL	0.725 ± 0.013	0.781 ± 0.009[b]	0.730 ± 0.008[b]
	7-PCSL	0.710 ± 0.011	0.751 ± 0.012[b]	0.715 ± 0.007[b]
PC/20 mol % DCP	5-SASL	0.678 ± 0.008	0.692 ± 0.012[c] 0.701 ± 0.010[d]	0.684 ± 0.009[e]
PC/20 mol % CL	5-SASL	0.658 ± 0.009	0.689 ± 0.010[c] 0.699 ± 0.011[d]	0.659 ± 0.009[e]

		h_{+1}/h_0	
system	probe	EGTA[a]	Ca^{2+}
SMP (1.0 mg of protein/mL)	5-MeSL	0.478 ± 0.008	0.445 ± 0.010[b]
SMP-extracted lipids[c]		0.668 ± 0.008	0.644 ± 0.012[e]

[a] At 1 mM. [b] At 5 mM. [c] At 8 mM. [d] At 12 mM. [e] At 10 mM.

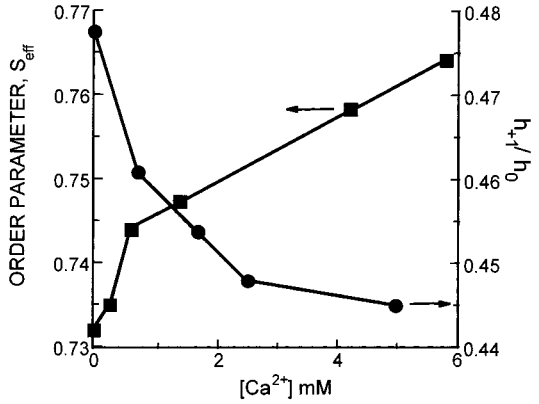

FIGURE 2: Ca^{2+} concentration dependence of SMP lipid organization. Spectral parameters S_{eff} (■) and h_{+1}/h_0 (●) determined from the EPR spectra of 5-SASL and 5-MeSL, respectively, incorporated in SMP (1.0 mg of protein/mL) in standard medium (see Materials and Methods) as a function of Ca^{2+} concentration.

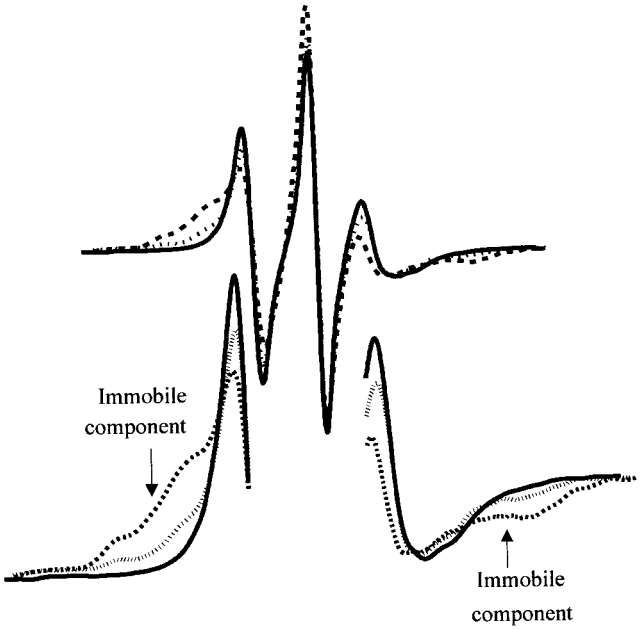

FIGURE 3: Effect of Ca^{2+} on SMP lipid acyl chain organization. (Top) EPR spectra of 12-SASL incorporated in SMP (2 mg of protein/mL) in the absence (···) and in the presence of 4 mM Ca^{2+} (- - -). For comparison, the spectrum of 12-SASL in PC/20 mol % CL liposomes is included (—). (Bottom) Enhancement of the low- and high-field regions of the spectra. The arrows denote the immobilized component in the spectra of SMP. This component is absent in the liposome spectra. Experimental conditions were as follows: power of 10 mW, modulation amplitude of 1.25 G, gain of 1.25×10^5, and spectral scan width of 100 G.

different packing properties. In contrast, in view of the greater fluidity in the terminal methyl region of the bilayer, the 12-doxyl derivative of stearic acid has a greater freedom of motion. In protein-containing membranes, probes carrying the nitroxide moiety close to the terminal methyl group exhibit two-component spectra; the narrow line component is ascribed to a more mobile lipid population, corresponding to bulk bilayer lipid, while the broader spectrum is ascribed to protein-bound, more immobilized, lipid (*13*, *31*). In Figure 3 (top), we compare the spectra of 12-SASL in PC/20 mol % DCP and in SMP, in the absence and presence of Ca^{2+}. Clearly, the spectra of the two latter systems exhibit at least two components, as found in studies of lipid−protein interactions. While a more immobilized component is absent

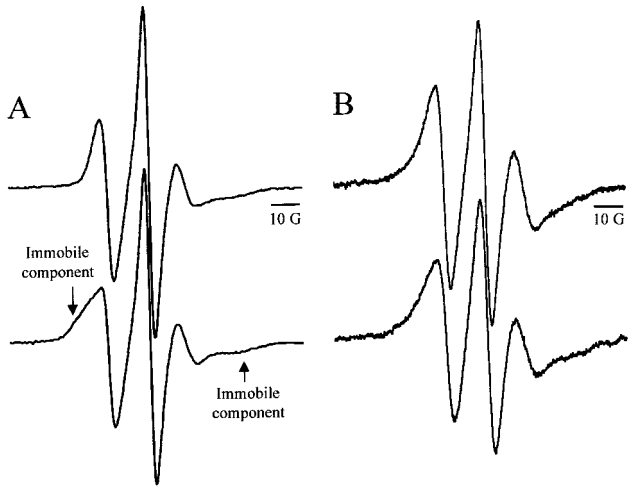

FIGURE 4: Effect of Ca^{2+} on SMP- and SMP-extracted lipid acyl chain organization. EPR spectra of 5-MeSL incorporated in SMP (2 mg of protein/mL) (A) and in liposomes of 8 mM SMP-extracted lipids (B), in standard medium in the absence (top) and in the presence of 4 mM (A) and 10 mM (B) Ca^{2+} (bottom). Experimental conditions were as follows: power of 10 mW, modulation amplitude of 1.25 G, gain of 1.25×10^5 (A) and 6.3×10^5 (B), and spectral scan width of 100 G.

in the spectra of the model membrane, it is present in spectra of SMP, and more so in those of Ca^{2+}-containing samples. These features are evidenced in Figure 3 (bottom), where the regions corresponding to the low- and high-field resonances were expanded.

A different behavior was observed for 5-MeSL, the methyl ester derivative of 5-SASL. When incorporated in SMP, this probe does not exhibit two-component spectra. Only a single spectrum, with no defined inner and outer extrema, is observed (Figure 4A, top), suggesting that this probe is not involved in lipid−protein interactions. Upon addition of Ca^{2+}, a broader component (denoted by the arrow in Figure 4A, bottom) appears, reflecting the formation of a more immobilized phase. The appearance of the Ca^{2+}-induced immobilized component causes a decrease in the ratio of the heights of the low-field (h_{+1}) to the midfield (h_0) resonance. Figure 2 shows that h_{+1}/h_0 decreases as the Ca^{2+} concentration increases. When added to SMP-extracted lipids, Ca^{2+} also caused a decrease of the h_{+1}/h_0 ratio in spectra of incorporated 5-MeSL (Table 1), indicating an increase in the extent of overall lipid organization (*28*). Nevertheless, in contrast to the results obtained for SMP, no additional spectral component was observed in this case (Figure 4B, bottom). Thus, the spectra of both 12-SASL and 5-MeSL, even at the low probe-to-lipid ratio, provided evidence for the formation of Ca^{2+}-induced, strongly immobilized, lipid domains in SMP.

EPR spectra of SMP, with high probe-to-lipid ratios, also allowed the assessment, at different depths in the bilayer, of Ca^{2+}-induced lipid domain formation. Figure 5 shows the EPR spectra of SSL in the absence (top) and in the presence (bottom) of Ca^{2+}. Line broadening due to the spin exchange interaction between the highly concentrated spin probes takes place both in the absence and in the presence of the ion. The exchange interaction increases in the latter case, indicating an increase in the local label concentration due to a redistribution of probe molecules in the plane of the membrane. Similar changes were found for a headgroup spin-

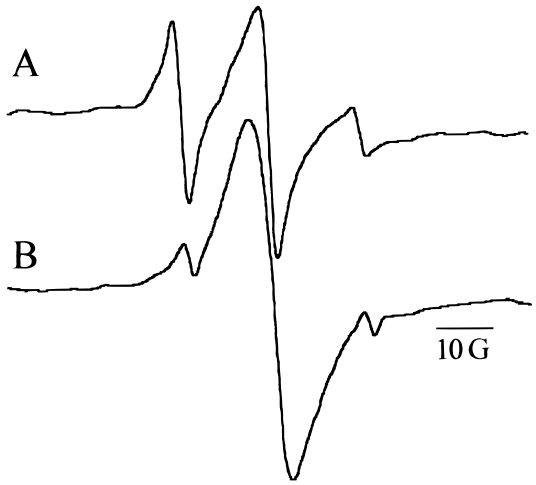

FIGURE 5: Ca^{2+}-induced lipid domain formation in SMP monitored by an increase of the exchange interaction at the headgroup level. EPR spectra of SSL (10 mol %) incorporated in SMP (1.0 mg of protein/mL) in standard medium (see Materials and Methods) in the absence (A) and in the presence (B) of 1.5 mM Ca^{2+}.

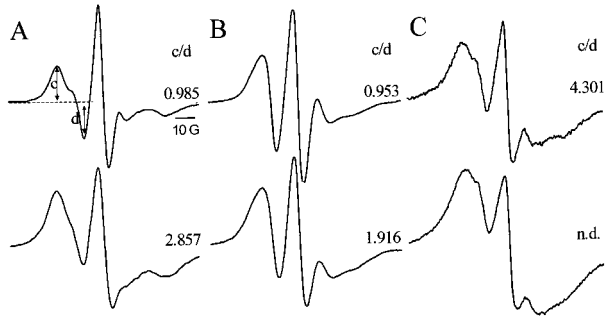

FIGURE 6: Effect of Ca^{2+} on lipid domain formation in SMP monitored in the acyl chain region. EPR spectra of (A) 5-SASL (10 mol %), (B) 5-MeSL (10 mol %), and (C) 7-PCSL (15 mol %) incorporated in SMP (1.0 mg of protein/mL) as described in Materials and Methods, in the absence (top) and in the presence of 1.5 mM (A) and 4.0 mM (B and C) Ca^{2+} (bottom). The measurement of *c* and *d* is denoted in panel A, and *c*/*d* ratios are given to the right of the spectra. Experimental conditions were as follows: power of 10 mW, modulation amplitude of 1.25 G, gain of 2.5×10^5 (A and B) and 3.2×10^5 (C), and spectral scan width of 100 G.

labeled derivative of palmitic acid when comparing mitochondria in the presence and in the absence of ATP (*32*).

The EPR spectra of 5-SASL-labeled SMP (Figure 6A) show that calcium also causes an increase in the exchange interaction. Estimation of line broadening, by the empirical *c*/*d* parameter (Figure 6; *28*), clearly indicates a higher Ca^{2+}-induced local label concentration. Similar results were obtained with 5-MeSL-labeled SMP (Figure 6B). An increase in the exchange frequency with increasing Ca^{2+} concentrations was also observed in the spectra of 7-PCSL (Figure 6C). Ca^{2+}-induced line broadening was observed to a smaller extent in the EPR spectra of 12-SASL-labeled SMP (not shown). This could be due to the fact that the propagation of the Ca^{2+}-induced effects decreases from the surface to the interior of the bilayer. It is worthwhile noticing that EGTA and Mg^{2+} were able to reverse the Ca^{2+}-induced line broadening in the spectra of all SMP-incorporated spin labels. In addition, Mg^{2+} alone did not produce spectral broadening, and the Ca^{2+}-promoted changes were unaltered upon addition of P_i in the 0.25−2 mM range. Moreover, Ca^{2+} exerted no

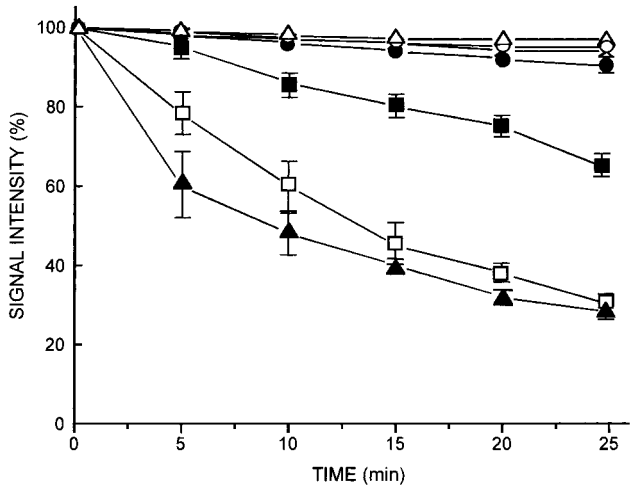

FIGURE 7: Disappearance of the nitroxide EPR spectra due to reaction with lipid peroxidation products formed upon addition of Ca^{2+} to SMP. Effect of Ca^{2+} on the kinetics of decay of the EPR signal of SSL, 5-SASL, and 12-SASL incorporated in SMP (1.5 mg of protein/mL). The nitroxides reacted with lipid peroxidation products resulting from respiration triggered by the addition of 10 mM succinate and 2.5 mM P_i. The standard medium (see Materials and Methods) contained 15 μM rotenone. (●) Control, nonrespiring SMP. The signal decay was very slow for all spin-labels; SSL in the presence of (○) 1.5 mM EGTA or (×) 5.5 mM Mg^{2+}. 5-SASL and 12-SASL yielded similar results. The remaining symbols correspond to systems with 1.5 mM Ca^{2+}: (■) SSL, (□) 5-SASL, (▲) 12-SASL, and (△) 12-SASL and 15 μM BHT. The values are the averages of four experiments.

effect when the spin labels were incorporated in nonrespiring mitoplasts (not shown). In these particles, the membranes are oriented right-side-out. Finally, Ca^{2+} failed to induce phase separation in PC/20 mol % CL/15 mol % 5-SASL liposomes (data not shown), in agreement with previously reported results (*16*).

Ca^{2+}-Promoted Lipid Peroxidation in Respiring SMP Monitored by the Kinetics of Spin Label Signal Decay and by Spin Trapping. Nitroxides are paramagnetic species; therefore, they can participate in free radical reactions, and the disappearance of the EPR signal can be used to probe these processes (*29*). Figure 7 summarizes the effect of Ca^{2+}, Mg^{2+}, BHT, and EGTA on lipid peroxidation in succinate-supplemented, antimycin A-poisoned SMP. The kinetics of the EPR signal decay were monitored for probes containing the nitroxide moiety at different depths in the bilayer. Addition of Ca^{2+} to SSL-labeled SMP resulted in a small signal loss during a period of 25 min. In contrast, the signal intensity decayed rapidly when SMP were labeled with 5-SASL and 12-SASL, whose paramagnetic groups are at a deeper location in the acyl chain region. These results demonstrate the dependence of the rate of spin label destruction on bilayer depth, suggesting that lipid-derived radicals are formed and that they react more effectively with 5-SASL and 12-SASL because of the location of the latter in the bilayer. Addition of BHT, an antioxidant, greatly inhibited the signal decay, demonstrating that the process is strictly related to lipid peroxidation. No significant signal loss occurred in the presence of EGTA, or in nonenergized SMP. In addition, substituting Ca^{2+} with Mg^{2+} prevented spin-label destruction.

ROS formation by mitochondria is a physiological event under aerobic conditions; the superoxide anion (O_2^-) is

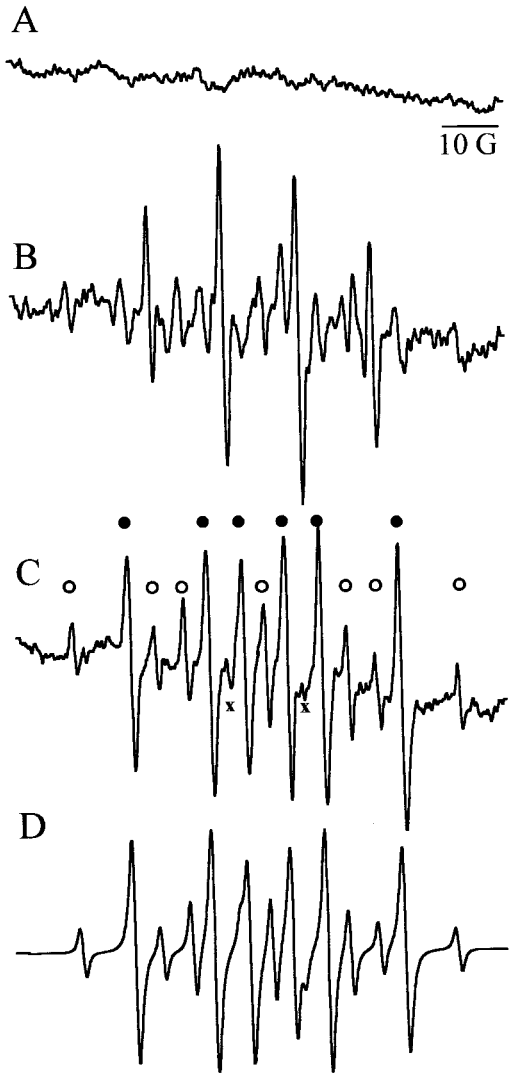

FIGURE 8: DMPO−spin adducts derived from SMP-generated ROS in the absence and in the presence of Ca^{2+}. EPR spectra of spin adducts obtained in succinate-supplemented SMP (3.5 mg of protein/mL) in standard medium containing 60 mM DMPO and 2.5 mM P_i in the presence of (A) 10 μM rotenone or 10 μM rotenone and 8 mM succinate and (B) 10 μM rotenone, 2 μM antimycin A, and 8 mM succinate. Under this condition, the spectrum of the DMPO−HO$^\bullet$ adduct is obtained; (C) same as panel B, with the results obtained after previous incubation with 2 mM Ca^{2+} for 15 min. Experimental conditions were as follows: scan time of 4 min, gain of 1.25×10^5, power of 20 mW, and modulation amplitude of 0.5 G. (D) Computer-simulated spectrum calculated with the hyperfine constants obtained in panel C, corresponding to DMPO spin adducts of H$^\bullet$ (○ and ×) and of a carbon-centered radical (●) (see the text).

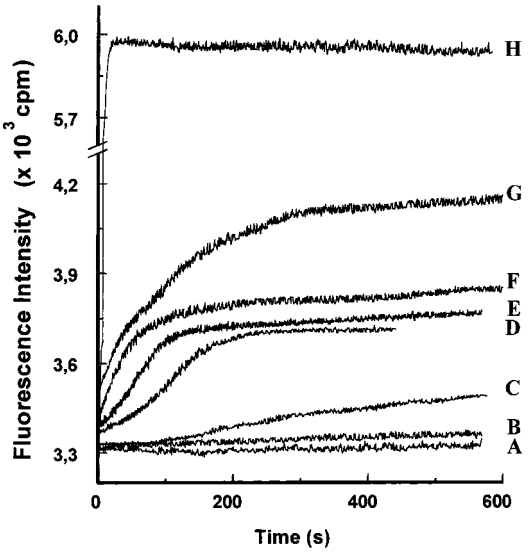

FIGURE 9: Carboxyfluorescein fluorescence as an indication of the Ca^{2+}-induced increase in SMP permeability. Effect of Ca^{2+} on a real-time measurement of fluorescence intensity (arbitrary units) of CF incorporated in the inner aqueous compartment of SMP (1.0 mg of protein/mL) in standard medium containing 1 μM antimycin A, 5 μM rotenone, and 2.5 mM P_i. The kinetic experiments were started by the addition of 5 mM succinate to SMP (A) in the absence of succinate and Ca^{2+} and in the presence of 0.2 mM EGTA, (B) in the presence of succinate and 0.2 mM EGTA, and (C) in the presence of 1 mM Ca^{2+} without succinate. Traces D−G correspond to succinate addition after a 10 min period of preincubation with 1, 3, 5, and 7 mM Ca^{2+}, respectively. (H) TX-100 was used to solubilize SMP to achieve total CF leakage.

produced, generating H_2O_2 and, probably, hydroxyl radicals (•OH) (*33*). Bovine heart SMP are also effective sources of O_2^- and H_2O_2 (*34*). Trapping of ROS upon reaction with DMPO provided direct evidence of Ca^{2+}-induced production of free radicals during SMP respiration. Figure 8 shows the effect of Ca^{2+} on the formation of DMPO adducts. No radical formation took place either under nonenergized conditions or when succinate was added to rotenone-containing SMP in the absence of antimycin A (Figure 8A). On the other hand, the •OH radical was formed by succinate-supplemented SMP in the presence of antimycin A (*34*, *35*), as seen in Figure 8B ($a_N = 14.9$ G, $a_H = 14.9$ G). Under this condition, the rate of O_2^- production increases, generating H_2O_2 by the noncatalyzed dismutation of the anion radical, since superoxide dismutase is also absent (*35*). The absence of catalase in SMP favors the increase in the level of H_2O_2 that can be consumed by cytocrome *c*, generating the highly reactive ferryl−heme species (*36*) and, in the presence of traces of iron, the •OH radical (*6*, *34*). The pattern of the EPR spectrum was modified in the presence of Ca^{2+} (Figure 8C), indicating the contribution of two main species: a carbon-centered radical−DMPO adduct [$a_N = 15.9$ G, $a_H = 22.9$ G (●)] and, to a lesser extent, the DMPO−H$^\bullet$ spin adduct [$a_N = 16.4$ G, $a_H = 22.5$ G (○); the x symbols denote lines overlapping with those of the carbon-centered radical]. The former values of hyperfine splittings are within the range reported for lipid-derived carbon-centered radical adducts (*37*). These radicals could originate from lipid peroxidation products formed by ROS attack on these membrane components. The formation of DMPO−H$^\bullet$ during lipid peroxidation has also been reported (*38*). BHT and EGTA prevented the appearance of the radicals. Figure 8D presents the simulated spectrum for the radicals identified in Figure 8C. It is seen that the agreement is excellent.

Ca^{2+}-Induced Increase in Membrane Permeability in Respiring SMP Monitored by Changes in the Fluorescence of Carboxyfluorescein Trapped in the Particle Internal Aqueous Compartment. Figure 9 shows no significant carboxyfluorescein (CF) leakage in SMP in the absence of succinate and Ca^{2+}. Addition of succinate to antimycin A-supplemented SMP in the absence of Ca^{2+} caused only a slight leakage of the dye. Under this condition, a Ca^{2+} concentration-dependent increase in the extent of CF leakage was observed. In the absence of antimycin A and succinate, Ca^{2+} also promoted an increase in permeability, characterized

by a lag phase, followed by an increase in fluorescence, but the effect was much less intense than that observed in the presence of succinate. Total leakage was induced by 0.2% TX-100. Despite the difficulty in removing the external CF from the SMP suspension, this method proved to be useful for detecting alterations in membrane permeability.

DISCUSSION

This work supports the hypothesis that the Ca^{2+}−CL interaction is one of the early events in the molecular mechanism of multiple membrane dysfunctions caused by Ca^{2+} overload in respiring mitochondria (*1*−*10*). The exposure of most of the CL (essentially the only negatively charged phospholipid of the IMM; *11*, *12*) to the external medium in SMP (*11*) allows for the examination of its interaction with externally added Ca^{2+}. The lack of significant changes in mitoplasts strongly suggests that in SMP Ca^{2+} binds considerably to CL. This lipid is tightly associated with several IMM enzymes, controlling their activities (*12*−*14*). Studies of reconstituted systems showed that cytochrome oxidase (COX) displays a higher affinity for CL than for other phospholipids, and that this affinity decreases in the presence of Ca^{2+} (*13*). In another study, removal of Ca^{2+} led to the loss of AAC channel activity (*20*). The Ca^{2+}-induced unselected channel activity was proposed to be a key component of the MTP pore.

In model systems, Ca^{2+} was shown to interact with CL's headgroup, causing a decrease in the surface area of monolayers and a consequent immobilization of the headgroups (*39*). In the study presented here, a Ca^{2+}-induced decrease of the motion of both the headgroup (Figure 1) and the acyl chain region (Figures 2−4), as well as an increase in the acyl chain degree of order (Figure 2 and Table 1), were observed in a biological membrane (SMP). Moreover, clear indications were found for Ca^{2+}-induced lipid lateral phase separation (Figures 5 and 6). Ca^{2+}-promoted increases in lipid order and lateral phase separation have been extensively examined in model membranes (*15*−*18*, *39*, *40*). Lateral phase separation was demonstrated by an increase in spin−spin interaction (*16*) and other experimental approaches (*17*, *18*, *40*). Nevertheless, this process was not characterized in PC/CL liposomes in this, or other studies (*16*, *41*). On the other hand, the Ca^{2+}-induced bilayer to hexagonal II phase transition described in PC/CL model systems (*15*, *39*, *42*) was not detected in this study, in agreement with previous work with biological membranes, including mitochondria (*42*), and with reconstituted membranes (*44*). In the IMM, the protein-to-lipid ratio is on the order of 80:20 (w/w). In spin label studies of lipid−protein interaction in COX-reconstituted systems, the spectral component due to nonboundary lipid exhibited broader line shapes with decreasing lipid content (*45*). The immobilization effect was seen to propagate to several lipid shells beyond that immediately adjacent to the protein. With regard to Ca^{2+}, the ion seems to compete with membrane proteins for CL, sequestering it from the boundary layer, as suggested by the decreased affinity of COX for spin-labeled CL in the presence of the ion (*13*), and by the loss of the AAC channel activity upon removal of Ca^{2+} (*20*).

In view of the above, the following sequence of events can be envisioned, at a molecular level. In SMP, essentially all the CL (∼20 mol %) is exposed to the external medium, and very likely, most of it is tightly bound to embedded proteins. Due to the low lipid-to-protein ratio, a large fraction of the lipid is directly involved in lipid−protein interactions. The remaining nonboundary lipids are also considerably immobilized, since in the IMM they comprise a small number of shells (*46*). This is best illustrated by the spectra of 5-MeSL. In the absence of Ca^{2+}, the probe exhibits essentially a single-component spectrum, indicating that it is not significantly involved in lipid−protein interactions. The empirical h_{+1}/h_0 parameter indicates that the SMP nonboundary lipid is more tightly packed than the extracted lipids (Figure 4 and Table 1). Upon addition of Ca^{2+}, CL is sequestered from the boundary lipid layer to the neighboring shells. Although Ca^{2+}-induced domain formation has not been observed in model systems containing CL (*16*, *41*), including this work, the phenomenon is clearly observed in SMP. Evidence for it is provided by the enhancement of spin exchange in spectra of SSL (Figure 5), 5-SASL, 7-PCSL, and 5-MeSL (Figure 6) at high probe-to-lipid ratios and from the increase of the strongly immobilized probe population in the spectra of SSL (Figure 1) and 12-SASL (Figure 3), as well as the appearance of such a population in the spectra of 5-MeSL (Figure 4A), at low probe-to-lipid molar ratios. The results for all probes, except 5-MeSL, do not allow ruling out the possibility of cluster formation in the boundary lipid domain. Nevertheless, the data for 5-MeSL, in conjunction with the above-mentioned results of Ca^{2+} effects on lipid−protein interactions in reconstituted systems (*13*, *20*), suggest that lateral phase separation occurs in the subsequent lipid shells, pointing at the different properties of this environment when compared to that of bulk bilayer lipids. In this context, Ca^{2+} sequestration of boundary layer CL would lead to an extensive rearrangement of the in-plane lipid distribution and packing within the membrane, promoting microdomain formation in the remaining lipid shells and creating packing defects between domains with different compositions. Moreover, the formation of Ca^{2+}−CL-enriched patches is expected not only to affect the lipid environment but also to influence the lateral motion of membrane proteins, as well as their conformation and function. In recent work on the interaction between cytochrome *c* and dimyristoylphosphatidylglycerol (DMPG), in the absence and presence of COX (*47*), the authors found that, whereas cytochrome *c* alone did not induce a motionally restricted population, it was able to increase the proportion of strongly immobilized lipid associated with COX/DMPG membranes. The results were proposed to be due to the propagation of the motional restriction of the lipid chains beyond the first boundary shell, possibly creating microscopic in-plane domains. It was also suggested that binding of cytochrome *c* might cause cross-bridging of COX molecules at lower lipid-to-enzyme ratios. Similar effects were found upon addition of melittin to sarcoplasmic reticulum membranes (*48*). The peptide-induced protein aggregation was suggested to be the main cause of the Ca^{2+}−ATPase inactivation.

The Ca^{2+}-promoted lateral phase separation, the packing defects between domains with different acyl chain mobility, and membrane protein aggregation are factors optimizing the topography for the efficient deleterious attack on IMM lipids and proteins by ROS. In fact, Ca^{2+} promotes an increased rate of carbon-centered radical production in succinate-

supplemented SMP (Figure 8C), strongly supporting this proposition. Formation of $HO^{\bullet}$ in succinate-supplemented SMP was demonstrated through the detection of the DMPO−OH adduct (Figure 8B). In the presence of Ca^{2+} and P_i, instead of this adduct, a carbon-centered radical is detected as a DMPO adduct (Figure 8C).

The physiological or stimulated production of mitochondrial O_2^{-}, after a period of anoxia and reoxygenation, and a consequent increase in the level of H_2O_2 have been observed (*6*, *9*, *33*−*36*). The absence of the DMPO−O_2^{-} adduct signal (a_N = 14.25 G, a_H = 11.3 G) does not exclude its participation, since this adduct is very unstable and decomposes to DMPO−OH (*37*). Like isolated mitochondria, SMP can give rise to H_2O_2. The production of H_2O_2 is enhanced several-fold in the presence of antimycin A (*34*, *35*). According to the proton-motive Q cycle hypothesis for electron transfer at the level of complex III (*49*), in the presence of antimycin A the ubisemiquinone radical accumulates on the cytosolic side of the IMM. Under this condition, production of superoxide has been ascribed to electron transfer to dioxygen either from the ubisemiquinone (*6*, *33*, *34*, *50*−*52*) or from cytochrome b_{566} (*53*).

Ca^{2+} induces a further increase in the levels of O_2^{-} and H_2O_2, leading to lipid and protein oxidation in intact mitochondria (*1*−*8*). The results presented here show that in the IMM, Ca^{2+} also stimulates free radical processes, probably by increasing the rate of production of H_2O_2 (*6*) and $HO^{\bullet}$ (*34*). The in-plane molecular rearrangement caused by the ion could facilitate the monovalent O_2 reduction, enhancing the generation of O_2^{-}, followed by H_2O_2 and other ROS. Moreover, the Ca^{2+}-induced lipid microstructural changes lead to at least two conditions favoring lipid and protein oxidation processes. (i) Increased lipid packing and lateral phase separation are known to enhance the propagation step of lipoperoxidation (*54*), generating secondary carbon-centered radicals (*9*, *37*). In this context, it is worthwhile noticing that CL contains highly unsaturated, oxidation prone, acyl chains (*12*). Therefore, the tight CL packing in the Ca^{2+}-induced clusters provides an environment that is favorable for faster propagation of the radical chain reaction (*54*). (ii) The rearrangement of protein components could also facilitate the exposition of target sites, leading to the observed extensive protein oxidation (*2*, *4*). Thus, Ca^{2+} sequestration of AAC tightly bound CL (*14*, *20*), and subsequent aggregation of the transporter, believed to be the main protein target for free radical attack (*1*, *2*, *4*), could promote the exposure of oxidizable SH groups, and intermolecular cross-linking. The detection of carbon-centered radicals in this study resembles the results obtained for myocardium submitted to ischemia/reperfusion (*37*), and reinforces the hypothesis that MPT is involved in tissue damage during reperfusion.

Ca^{2+}-induced lipid peroxidation in respiring SMP was also monitored by the kinetics of nitroxide EPR signal loss (Figure 7) due to the reaction of this moiety with lipid-derived radicals (*29*). The faster rate in the acyl chain region indicates that labels in a hydrophobic environment are more accessible than those at the membrane−water interface (Figure 7), suggesting that the formation of primary radicals and propagation of oxidation occur mainly in the SMP hydrophobic core. As previously demonstrated for mitochondria (*1*, *3*−*8*), oxidative stress causes a marked increase in SMP permeability (Figure 9), in agreement with ΔpH measurements that indicate disruption of the SMP transmembrane potential (data not shown). The phase separation characterized in this work causes changes in the lipid microenvironment that are sufficient to cause a significant increase in permeability, as observed for liposomes (*40*, *42*). However, only under conditions of radical overproduction, occurring in antimycin A-poisoned, succinate-supplemented SMP, is there a pronounced Ca^{2+} concentration-dependent permeability increase. In the presence of high calcium, the SMP respiration process leads to an increase in H_2O_2 formation, triggering the oxidative process. Taken in conjunction, the results presented here show that Ca^{2+} has multiple effects. The Ca^{2+}−SMP interaction, mediated by Ca^{2+}−CL binding, is a precondition that favors a sequence of inter-related structural, dynamical, and chemical events. The decreased lipid mobility and increased order, the formation of CL-enriched domains, interdomain packing defects, and protein aggregation are structural−dynamical events that can induce and/or favor deleterious chemical processes modulated by the reorganization of membrane components. This rearrangement leads to increased ROS production at the ubiquinone level, promoting the oxidation of membrane lipids and proteins whose chemical damage is responsible for the large increase in membrane permeability. Altogether, the data strongly indicate that the Ca^{2+}−CL interaction is an early and fundamental step of the molecular mechanism by which Ca^{2+} triggers mitochondrial membrane permeabilization. The above sequence of events provides an explanation for the IMM nonspecific permeability transition observed at high Ca^{2+} concentrations.

ACKNOWLEDGMENT

We are indebted to Drs. O. Augusto and J. V. Vivar, and to Ms. L. S. Nakao for valuable discussions and help in the analysis of the spin trapping data.

REFERENCES

1. Zoratti, M., and Szabò, I. (1995) *Biochim. Biophys. Acta 1241*, 139−176.
2. Fagian, M. M., Pereira-da-Silva, L., Martins, I. S., and Vercesi, A. E. (1990) *J. Biol. Chem. 265*, 19955−19960.
3. Kowaltowski, A. J., Castilho, R. F., Grijalba, M. T., Bechara, E. J. H., and Vercesi, A. E. (1996) *J. Biol. Chem. 271*, 2929−2934.
4. Halestrap, A. P., Woodfield, K.-Y., and Connern, C. P. (1997) *J. Biol. Chem. 272*, 3346−3354.
5. Vercesi, A. E., Kowaltowski, A. J., Grijalba, M. T., Meinicke, A. R., and Castilho, R. F. (1997) *Biosci. Rep. 17*, 43−52.
6. Kowaltowski, A. J., Castilho, R. F., and Vercesi, A. E. (1995) *Am. J. Physiol.*, C141−C147.
7. Kowaltowski, A. J., Netto, L. E. S., and Vercesi, A. E. (1998) *J. Biol. Chem. 273*, 12766−12769.
8. Novgorodov, S. A., Gudz, T. I., Brierley, G. P., and Pfeiffer, D. R. (1989) *Arch. Biochem. Biophys. 311*, 219−228.
9. Ambrosio, G., Zweier, J. L., Duilio, C., Kuppusamy, P., Santoro, G., Elia, P. P., Trito, I., Cirillo, P., Condorelli, M., Chiarello, M., and Flaherty, J. T. (1993) *J. Biol. Chem. 268*, 18532−18541.
10. Greene, E. L., and Paller, M. S. (1994) *Am. J. Physiol. 266*, F13−F20.
11. Harb, J. S., Comte, J., and Gautheron, D. C. (1980) *Arch. Biochem. Biophys. 208*, 305−318.
12. Hoch, F. L. (1992) *Biochim. Biophys. Acta 1113*, 71−133.
13. Powell, G. L., Knowles, P. F., and Marsh, D. (1987) *Biochemistry 26*, 8138−8145.

14. Beyer, K., and Klingenberg, M. (1985) *Biochemistry 24*, 3826−3831.
15. De Kruijff, B., Verkleij, A. J., Leunissen-Bijvelt, J., Van Echteld, C. J. A., Hille, J., and Rijnbout, H. (1982) *Biochim. Biophys. Acta 693*, 1−12.
16. Ohnishi, S., and Ito, T. (1974) *Biochemistry 13*, 881−887.
17. Haverstick, D. M., and Glaser, M. (1987) *Proc. Natl. Acad. Sci. U.S.A. 84*, 4475−4479.
18. Lieser, G., Mittler-Nehar, S., Spinke, J., and Knoll, W. (1994) *Biochim. Biophys. Acta 1192*, 14−20.
19. Edidin, M. (1997) *Curr. Opin. Struct. Biol.*, 582−532.
20. Brustovetsky, N., and Klingenberg, M. (1996) *Biochemistry 35*, 8483−8488.
21. Vercesi, A. E., Reynafarje, B., and Lehninger, A. L. (1978) *J. Biol. Chem. 253*, 6379−6385.
22. Beltran, C., Gomez-Puyou, M. T., Darzon, A., and Gomez-Puyou, A. (1986) *Eur. J. Biochem. 160*, 163−168.
23. Rouser, G., Fleischer, S., and Yamamoto, A. (1970) *Lipids 5*, 494−496.
24. Lowry, O. H., Rosebrough, N. J., Farr, A. L., and Randall, R. S. (1951) *J. Biol. Chem. 193*, 265−275.
25. Folch, J., Lees, M., and Sloane-Stanley, G. H. (1957) *J. Biol. Chem. 226*, 497−501.
26. Hubbell, W. L., and McConnell, H. M. (1971) *J. Am. Chem. Soc. 93*, 314−326.
27. Schreier, S., Polnaszek, C. F., and Smith, I. C. P. (1978) *Biochim. Biophys. Acta 515*, 375−436.
28. Frezzatti, W. A., Jr., Toselli, W. R., and Schreier, S. (1986) *Biochim. Biophys. Acta 860*, 531−538.
29. Grijalba, M. T., Andrade, B. A., Meinicke, A. R., Castilho, R. F., Vercesi, A. E., and Schreier, S. (1998) *Free Radical Res. 28*, 301−318.
30. Schreier, S., Marsh, D., and Smith, I. C. P. (1976) *Arch. Biochem. Biophys. 172*, 1−11.
31. Jost, P. C., Griffith, O. H., Capaldi, R. A., and Vanderkooi, G. (1973) *Proc. Natl. Acad. Sci. U.S.A. 70*, 480−484.
32. Koltover, V. K., Reichman, L. M., Yasaitis, A. A., and Blumenfeld, L. A. (1971) *Biochim. Biophys. Acta 234*, 306−310.
33. Cadenas, E. A., Boveris, A., Ragan, C. I., and Stoppani, A. O. M. (1977) *Arch. Biochem. Biophys. 180*, 248−257.
34. Giulivi, C., Boveris, A., and Cadenas, E. (1995) *Arch. Biochem. Biophys. 316*, 909−916.
35. Boveris, A., Cadenas, E. A., and Stoppani, A. O. M. (1976) *Biochem. J. 156*, 435−444.
36. Radi, R., Sims, S., Cassina, A., and Turrens, J. F. (1993) *Free Radical Biol. Med. 15*, 653−659.
37. Arroyo, C. M., Kramer, J. H., Dickens, B. F., and Weglicki, W. B. (1987) *FEBS Lett. 221*, 101−104.
38. Makino, K., Imaishi, H., Morinishi, S., Takeuchi, T., and Fujita, Y. (1986) *Biochem. Biophys. Res. Commun. 141*, 381−386.
39. Killian, J. A., Koorengevel, M. C., Bouwstra, J. A., Gooris, G., Dowhan, W., and de Kruijff, B. (1994) *Biochim. Biophys. Acta 1189*, 225−232.
40. Mittler-Neher, S., and Knoll, W. (1993) *Biochim. Biophys. Acta 1152*, 259−269.
41. Cable, M. B., and Powell, G. L. (1980) *Biochemistry 19*, 5679−5686.
42. Smaal, E. S., Schreuder, C., van Baal, J. B., Tijburg, P. N. M., Mandersloot, J. G., de Kruijff, B., and de Gier, J. (1987) *Biochim. Biophys. Acta 897*, 191−196.
43. de Kruijff, B., Nayar, R., and Cullis, P. R. (1982) *Biochim. Biophys. Acta 684*, 47−52.
44. Taraschi, T. F., de Kruijff, B., and Verkleij, A. J. (1983) *Eur. J. Biochem. 129*, 621−625.
45. Knowles, P., Watts, A., and Marsh, D. (1979) *Biochemistry 18*, 4480−4487.
46. Marsh, D., Watts, A., Maschke, W., and Knowles, P. (1978) *Biochem. Biophys. Res. Commun. 81*, 397−402.
47. Kleinschmidt, J., Powell, G. L., and Marsh, D. (1998) *Biochemistry 37*, 11579−11585.
48. Mahaney, J. E., Kleinschmidt, J., Marsh, D., and Thomas, D. D. (1992) *Biophys. J. 63*, 1513−1522.
49. Trumpower, B. L. (1990) *J. Biol. Chem. 265*, 11409−11412.
50. Turrens, J. F., Alexander, A., and Lehninger, A. L. (1986) *Arch. Biochem. Biophys. 237*, 408−414.
51. Skulachev, V. P. (1996) *FEBS Lett. 397*, 7−10.
52. Zhang, L., Yu, L., and Yu, C.-A. (1998) *J. Biol. Chem. 273*, 33972−33976.
53. Nohl, H., and Jordan, W. (1986) *Biochem. Biophys. Res. Commun. 138*, 533−539.
54. Verstraeten, S. V., Nogueira, L. V., Schreier, S., and Oteiza, P. I. (1997) *Arch. Biochem. Biophys. 338*, 121−127.

BI9828674